



Double Electron–Electron Resonance vs. Instantaneous Diffusion Effect on Spin-Echo for Nitroxide Spins Labels

Elena A. Golysheva¹ · Anna S. Smorygina¹ · Sergei A. Dzuba^{1,2} 

Received: 3 May 2021 / Revised: 28 June 2021 / Accepted: 7 July 2021 /

Published online: 18 July 2021

© The Author(s), under exclusive licence to Springer-Verlag GmbH Austria, part of Springer Nature 2021

Abstract

Double electron–electron resonance (DEER, also known as PELDOR) is an efficient tool to study nanoscale distances between paramagnetic species forming oligomers or arranged in clusters. DEER also may be applied to study heterogeneous systems in which large clusters of spin labels may be considered as randomly distributed species of enhanced local concentration. For these systems, information of the same kind could be obtained with a simple two-pulse Hahn’s spin-echo sequence, if a so-called instantaneous diffusion (ID) effect is separated from other dephasing processes. Comparison of DEER and ID decays performed here at X-band EPR for model systems of nitroxides dissolved in molecular glasses showed good agreement between DEER and ID data, as well as with theory for randomly distributed spins. For spin-labeled stearic acids in a model biological membrane, the obtained DEER and ID data indicate on cluster formation with enhanced local concentration. For high stearic acid concentration, the ID data were found to strongly deviate from the DEER data, which were interpreted as an evidence for correlation of mutual orientations of spin labels in the clusters.

1 Introduction

Double electron–electron resonance (DEER), also known as pulsed electron double resonance (PELDOR) [1–3], is widely used for studying distances between paramagnetic species in the nanoscale range [4–11]. The DEER signal is induced by the dipolar interaction of the spin labels in the biradical or oligomer (cluster) under investigation and a background contribution caused by the surrounding spins in other molecules or clusters.

✉ Sergei A. Dzuba
dzuba@kinetics.nsc.ru

¹ Voevodsky Institute of Chemical Kinetics and Combustion, Russian Academy of Sciences, Novosibirsk, Russia

² Department of Physics, Novosibirsk State University, Novosibirsk, Russia

The DEER technique is applicable if the spin system can be separated into two subsystems, named A and B, possessing two different resonance frequencies, ν_A and ν_B ; most commonly both subsystems are composed of the same type of spin labels and differ only due to g -tensor and hyperfine interactions. Then, the electron spin-echo (ESE) signal arising from spins A may be affected by application of an additional pumping pulse acting on spins B, because this pulse instantaneously modulates the dipole–dipolar (d–d) interaction between two spins.

In the case of simple two-pulse Hahn’s ESE formation, the d–d interaction between spins is also modulated, because the second echo-forming pulse, in addition to its common refocusing action, acts in a way similar to the pumping pulse in DEER—it modulates instantaneously the d–d interactions. This modulation affects spin precession. To distinguish this modulation from thermally activated spectral diffusion, the instant influence by pulse modulation is called “instantaneous” diffusion [12] (ID). The ID effect on the ESE signal is the same as the pumping pulse influence on DEER signal, with the difference only that, in ID, the spins A and B possess close resonance frequencies.

The difference however may become crucial when this condition cannot be fulfilled, which, e.g., may take place when two interacting spins are specifically oriented, so that they cannot be simultaneously excited. Another serious drawback of the simple two-pulse ESE approach in studying d–d interactions is the dead-time problem which prevents signal detection at small interpulse delays; at X-band EPR, the dead-time is typically around 100 ns. These two drawbacks of ID experiment do not allow studying distance distributions between two spins in the pair which is the main advantage of DEER experiment.

However, these two drawbacks of ID experiment become unimportant in the case of spin labels randomly distributed and randomly oriented in the space, because, first, different orientations are available for excitation and detection, and, second, theory predicts in this case exponential decay which allows extrapolation to the zero time. For three–dimensional (3D) spatial distribution, theory [13] predicts that echo decay due to the ID mechanism is described by

$$E_{3D}(\tau) = E_0 \exp\left(-\frac{8\pi^2}{9\sqrt{3}} \frac{g^2 \mu_B^2}{\hbar} C p_A \tau\right), \quad (1)$$

where g is the g -factor, μ_B is the Bohr magneton, C is the volume spin concentration, p_A is the excitation efficiency of the second echo-forming pulse (see below), and τ is the time delay between two pulses. For the DEER signal, the similar relation holds, with only two differences: the p_A factor is replaced by the excitation efficiency of the pumping pulse p_B , and time delay τ is replaced by time delay T of the pumping pulse [14]

$$E_{3D}(T) = E_0 \exp\left(-\frac{8\pi^2}{9\sqrt{3}} \frac{g^2 \mu_B^2}{\hbar} C p_B T\right). \quad (2)$$

For two-dimensional (2D) space distribution which takes place, e.g., for spin-labeled molecules in biological membranes, theory [14, 15] predicts that signal is proportional to the factor of $\exp(-\text{const} \times \sigma p_A \tau^{2/3})$ (or correspondingly to $\exp(-\text{const} \times \sigma p_B T^{2/3})$), where σ is the surface spin concentration. Simulations taking into account averaging over all the plane orientations in the space [16] showed that in this case

$$E_{2D}(\tau) \cong E_0 \exp\left(-3.21 \sigma p_A (g^2 \mu_B^2 \tau / \hbar)^{\frac{2}{3}}\right), \quad (3)$$

for the ID mechanism of echo decay, and

$$E_{2D}(T) \cong E_0 \exp\left(-3.21 \sigma p_B (g^2 \mu_B^2 T / \hbar)^{\frac{2}{3}}\right), \quad (4)$$

for the DEER signal.

One can see that time dependences for both the ID and DEER experiments [cf. Eqs. (1) and (2), Eqs. (3) and (4)] look very similar. From these dependencies, the concentrations C or σ may be obtained. These concentrations may become useful information when studying systems in which nanoscopic heterogeneity is expected; then, they are to be denoted as local concentrations, C_{loc} and σ_{loc} . These concentration indeed refer to heterogeneities of nanoscale size, evaluated as $r \sim (g^2 \mu_B^2 T / \hbar)^{1/3}$, that is several nm for typical T (or τ) values, lying for organic solids in the microsecond time scale.

Such heterogeneities were detected using the ID effect for free radicals trapped in irradiated solids [17–20], for spin-labeled biomolecules encapsulated in mesoporous materials [21] and attached to cotton fibers [22], for molecular nano-clusters formed in biological membranes [23–26], for defects in metal–organic frameworks [27], for high-spin organic materials [28]. As compared with DEER applications, in certain cases, ID experiment may become preferable, because, first, DEER measurements require more sophisticated instrumentation and, second, theory of DEER effect in some cases may become rather complicated [29].

One may suggest that comparison of these two types of experiment—ID and DEER—may reveal important details of the mutual spin label distribution. In this work, to make this comparison more reliable, we start with a well-characterized model system in which random distribution of spin labels is *a priori* expected: that is nitroxides dissolved in molecular glasses. Good agreement found between ID and DEER data for these systems additionally confirms validity of the general description given by Eqs. (1) and (2). However, upon transition to a more complicated system—spin-labeled stearic acids clustered in model biological membranes—we found remarkable disagreement between the two data sets. We show that this disagreement may become a source of additional information on properties of the spin-labeled clusters under investigation.

To analyze the ID and DEER experiments, the $p_{A(B)}$ parameter in Eqs. (1) – (4) should be assessed. It is given by averaging over the excited EPR spectrum [13]

$$p_{A(B)} = \int g(\nu) d\nu \frac{\nu_1^2}{(\nu_{A(B)} - \nu)^2 + \nu_1^2} \sin^2 \left(\pi t_p \sqrt{(\nu_{A(B)} - \nu)^2 + \nu_1^2} \right), \quad (5)$$

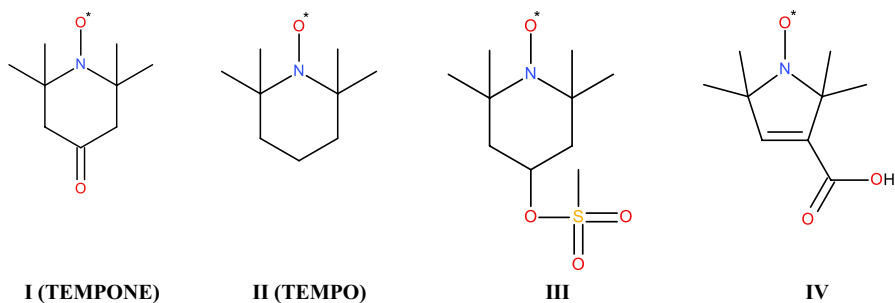
where ν_1 and t_p are the second microwave pulse (ID experiment) or pumping pulse (DEER experiment) amplitude and duration, respectively, $g(\nu)$ is the EPR spectral line shape. The $g(\nu)$ function is assumed to be normalized, $\int g(\nu) d\nu = 1$. Inspection of Eq. (5) shows that if ν_1 is smaller than the EPR spectral width, then p_A becomes smaller with smaller t_p value (with ν_1 keeping constant). Also, in this case, $p_{A(B)}$ is proportional to the spectral amplitude $g(\nu_{A(B)})$. Therefore, there are two ways to change $p_{A(B)}$ value: either by changing the pulse parameters or by shifting the excited spectral position.

2 Experimental

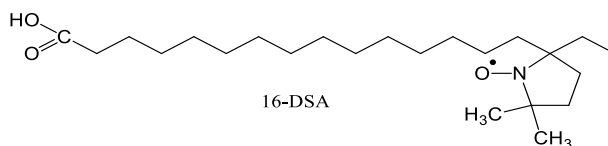
2.1 Materials and Samples

Four nitroxide free radicals (Scheme 1) were used. Nitroxides **I** and **II** were purchased from Sigma-Aldrich (Saint Louis, MO, USA) and used without further purification. Nitroxides **III** and **IV** were from Reanal (Budapest, Hungary) and were purified by recrystallization from toluene; their melting points after purification were 90 °C and 210 °C, which are in good agreement with the literature data (91–92 °C for **III** [30] and 210 °C for **IV** [31]). The lipids 1,2-dipalmitoyl-*sn*-glycero-3-phosphocholine (DPPC), 1,2-dioleoyl-*sn*-glycero-3-phosphocholine (DOPC) were obtained from Avanti Polar Lipids (Birmingham, AL, USA); spin-labeled 16-doxyl-stearic acid (16-DSA) (Scheme 2), glycerol, and OTP were purchased from Sigma-Aldrich (Saint Louis, MO, USA); these substances were used without purification.

Nitroxides were dissolved either in water-glycerol mixture (50:50 w/w, abbreviated below as WG) at room temperature or in ortho-terphenyl (OTP) at elevated temperatures of 56 °C or 130 °C (in the case of nitroxide **IV**). The sample preparation looked as follows. First, 1 mg of nitroxide was dissolved in the required amount of solvent to achieve concentration of 6 mM. Then, other concentrations were obtained



Scheme 1 Chemical structures of nitroxides in this study



Scheme 2 Chemical structure of 16-doxyl-stearic acid (16-DSA)

by calibrated dilution. After mixing on a Bio Vortex V-1 (Biosan, Latvia), all samples were frozen in liquid nitrogen to obtain a transparent glass.

For preparation spin-labeled model membranes, DPPC and DOPC lipids taken in equimolar amount and the required amount of 16-DSA were dissolved separately in chloroform and then the solutions were mixed. Chloroform was then removed in nitrogen stream, with the remaining powder subsequently stored under vacuum for 4 h. Then, phosphate-buffered saline (PBS) was added to the powder in a proportion 10:1, and the resulting sample was stored for 2 h at room temperature and then centrifuged to remove the excess solvent. Upon this procedure, multilamellar vesicles (MLV) were formed.

2.2 Measurements

All experiments were carried out on an X-band ELEXSYS 9-GHz FT-EPR spectrometer (Bruker, Bremen, Germany) equipped with a CF 935 cryostat (Oxford instruments, Abingdon, UK). A dielectric resonator (Bruker ER 4118X-MD5) was used for obtaining CW EPR spectra. CW EPR experimental parameters were chosen to avoid saturation and overmodulation. Pulse experiments were conducted with a split-ring Bruker ER 4118X-MS3 resonator which was overcoupled to provide a ringing time of about 100 ns.

CW EPR spectra were recorded at 150 K for WG samples and at 200 K for samples with OTP. All pulse experiments were carried out at 80 K. The temperature was controlled by a cold nitrogen stream with an accuracy of ± 0.5 K.

ID was studied with two-pulse sequence ($90^\circ\text{-}\tau\text{-}180^\circ\text{-}\tau\text{-echo}$). The pulse durations were 16 ns and 32 ns for the 90° and 180° pulses, respectively. The time delay τ was scanned from 120 ns with steps either of 4 ns, or 8 ns, or 12 ns. Echo-detected (ED) EPR spectra were recorded with two-pulse sequence when τ was kept constant at 120 ns.

A three-pulse DEER pulse scheme was used with the phase correction suggested in [32] to prevent signal distortion upon passage the pumping pulse through the detection pulses. The two-pulse echo-forming sequence was the same ($90^\circ\text{-}\tau\text{-}180^\circ\text{-}\tau\text{-echo}$) as for the ID experiment. The time delay τ was kept constant, either 2 μs or 0.8 μs . The pumping pulse was a 180° pulse with duration of 32 ns. The frequency ν_B of the pumping pulse corresponded to excitation of the maximum of the echo-detected EPR spectrum, and the difference $\nu_A\text{-}\nu_B$ between the detection and pumping frequencies was set either near 90 MHz which corresponded to detection on the right spectral shoulder or at -70 MHz which corresponded to detection on the left spectral shoulder. In some cases, $\nu_A\text{-}\nu_B$ was set between 40 and 90 MHz. The time

delay between the first detection pulse and the pumping pulse, T , was scanned starting from a negative value of -200 ns, with the time step either of 4 ns, or 8 ns, or 12 ns.

3 Results and Discussion

3.1 Nitroxides in Molecular Glasses

CW EPR spectra recorded at low temperatures for nitroxides of different concentrations in WG and OTP glasses are shown in Fig. 1. These spectra are typical for immobilized nitroxides. One can see that spectra of I–III are almost independent of concentration. For nitroxide IV in OTP glass, for concentrations larger than 2 mM, one may notice however appearance of additional lines. This spectral change may indicate dimerization of nitroxides. We may point out that this nitroxide possesses a high polarity (see Scheme 1), so that dimerization of the “head-to-tail” type can be a natural process to diminish the total electric dipolar moment of nitroxides in a non-polar OTP matrix.

To analyze the ID effect in the echo decays, one has to take into account that echo decays due to several different mechanisms, induced not only by ID but also by stochastic spectral diffusion (spin diffusion in the surrounding nuclear subsystem, etc.). To separate the ID effect, one may employ its dependence on the turning angle and on the spectral density at the resonance frequency position as was described above: by changing either the pulse parameters or the spectral position with different spectral density $g(\nu_A)$. Note that another possible mechanism of echo decay which depends on $g(\nu_A)$ is stochastic molecular librations; however, at the temperature of our experiment (80 K), this mechanism was shown to be ineffective [33, 34].

Hence, the contribution of ID can be easily extracted by comparison of the echo decays obtained either with two different second microwave pulse durations [for example, with the conventional pulse sequence $90^\circ\text{-}\tau\text{-}180^\circ\text{-}\tau\text{-echo}$, denoted below as $E_1(\tau)$ and with the $90^\circ\text{-}\tau\text{-}90^\circ\text{-}\tau\text{-echo}$ pulse sequence ($e_1(\tau)$], or at two field positions with two different $g(\nu_A)$ spectral density, denoted here as $E_1(\tau)$ and $E_2(\tau)$. Below, we refer to these two types of ID extraction as ID experiments of the 1st and the 2nd kinds, correspondingly.

An example of these two ID experiments is presented in Fig. 2 in a semi-logarithmic plot. The insert to Fig. 2a shows how spins are excited in different experiments (the field positions 1, 2, and 3). In Fig. 2a, the original decays are shown; one can notice some nonlinearity of the curves which means non-exponential decays. Also, some oscillations on the decay curve are seen; these oscillations may be unambiguously ascribed to ESE envelope modulation (ESEEM) effect induced by hyperfine interaction with proton matrix. The ratios of these ESE decays [$\ln(E_1(\tau)/e_1(\tau))$ refers to the ID experiment of the 1st kind and $\ln(E_1(\tau)/E_2(\tau))$ to that of the 2nd kind] become linear in the logarithmic scale (Fig. 2b) which implies an exponential behavior predicted by Eq. (1). Also, the ESEEM effects are suppressed after division. In Fig. 2b, the DEER signal decays are also given, obtained at the detecting positions 2 and 3.

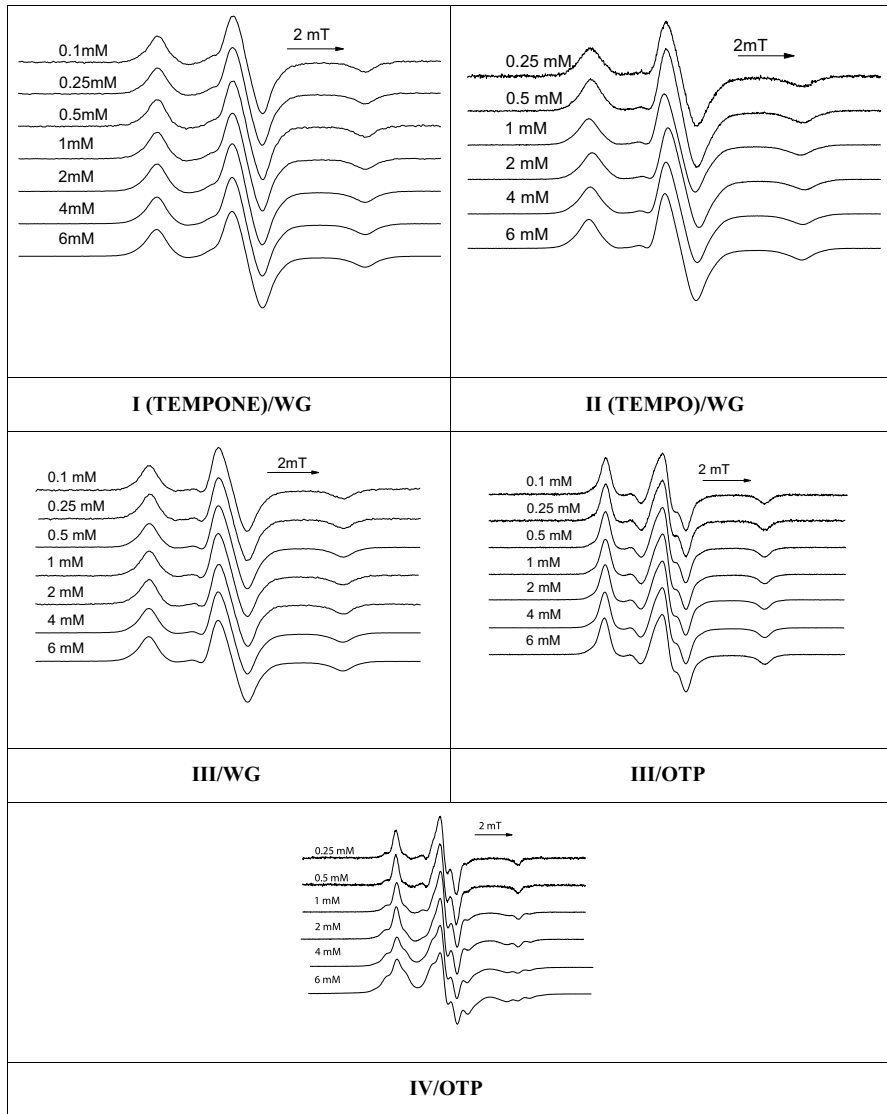


Fig. 1 CW EPR spectra recorded at 150 K for WG and at 200 K for OTP glasses. The spectra are normalized to the central peak and vertically shifted for better presentation

It can be seen from Fig. 2b that comparison of ESE decays at two field positions (the 2nd kind of the ID extraction) gives more pronounced effect than that for the ESE decays at the same field position but with different second pulse duration (the 1st kind of ID experiment). The DEER signal decays even more rapidly (see “Discussion” below). Quantitatively, the tangents obtained from data in Fig. 2b are 0.34 , 1.08 , and $1.45 \mu\text{s}^{-1}$ for the two kinds of ID and DEER measurements, correspondingly, which makes the proportion $0.23:0.74:1$. DEER data obtained at the

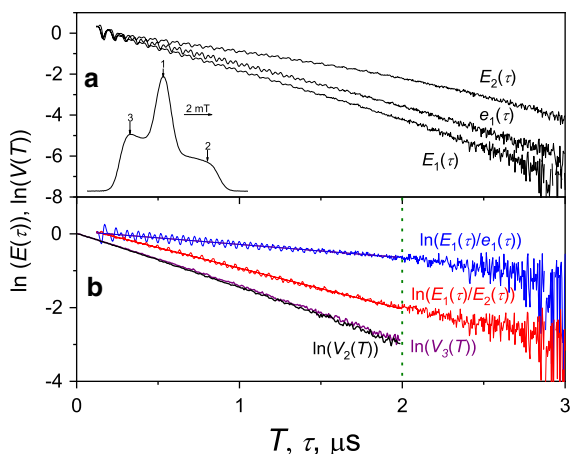
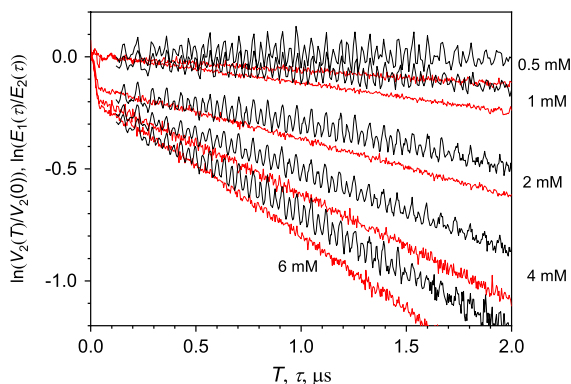


Fig. 2 **a** Echo decays given in a semi-logarithmic plot obtained at the field position 1 (see insert) with the pulse sequences $90^\circ\text{-}\tau\text{-}180^\circ\text{-}\tau\text{-echo}$ ($E_1(\tau)$) and $90^\circ\text{-}\tau\text{-}90^\circ\text{-}\tau\text{-echo}$ ($e_1(\tau)$) and at the field position 2 obtained with the pulse sequence $90^\circ\text{-}\tau\text{-}180^\circ\text{-}\tau\text{-echo}$ ($E_2(\tau)$). **(b)** The ratios of these decays; the straight lines are linear approximations in the time range limited by the vertical dotted line. In addition, the DEER signals, $\ln(V_3(T))$ (purple line) and $\ln(V_2(T))$ (black line), are given (the observation is at the spectrum positions 3 and 2, respectively). The sample is 6 mM nitroxide **I** (TEMPONE) in WG glass, and the lines are vertically shifted for the clarity of presentation (Color figure online)

field positions 2 and 3 (detection at the right and left spectral shoulders) provided similar results.

Figure 3 shows DEER and ID time traces obtained for nitroxide **IV** in OTP glass. With increasing concentration, DEER data show a remarkable signal drop at time delays below 50 ns (modulation of DEER signal) which unambiguously may be ascribed to the dimerization process that was discussed above. After 50 ns, DEER signal decays exponentially, which is in agreement with Eq. (2); this decay is called a background DEER signal. For ID decays, because of the dead-time problem, this modulation is missed. However, one can notice that ID decays are in good agreement with the background DEER signal.

Fig. 3 The ID decays (black oscillating curves) and DEER time dependences (red curves, observation at the 2nd field position) for nitroxide **IV** in OTP. The ID data were obtained by comparing decays at the field positions 1 and 2 (ID experiment of the 2nd kind). ID data are shifted downwards to match the DEER data (Color figure online)



The ID and DEER data for the other studied samples are shown in Fig. 4, also in a semi-logarithmic plot. All ID data shown were obtained in ID experiment of the 2nd kind. In DEER experiments, the pumping pulse was applied at position 1 with observation at position 3. For better visualization of comparison with theoretical equations [Eqs. (1) and (2)], all data in Fig. 4 are divided by the nitroxide concentrations (taken in mM units). One can see that data may be approximated by straight lines, parallel to each other, which is in agreement with theory. Note that DEER data do not show dimerization like it is observed for **IV** (cf. Fig. 3)—because the initial fast drop at the beginning is absent here.

One can see that the slopes of the ID time dependences in Figs. 2, 3 and 4 are systematically smaller than those for the DEER experiment. This has a simple explanation: according to Eqs. (1) and (2), the tangent of slope for DEER decay is proportional to the $p_B \equiv p_1$ value where subscript “1” denotes excitation at the position 1 in the EPR spectrum (see insert to Fig. 2a), while the tangent of slope for ID decay is proportional to the difference $p_1 - p_2$ where subscript “2” denotes excitation at the position 2, with $p_A \equiv p_2$; for both kinds of experiments, the p_1 value may be considered the same (see Experimental). Then, comparison of experimental time traces, e.g., for nitroxide I (TEMPONE) in WG glass at 1 mM concentration (see Fig. 4) with Eq. (2) for DEER data provides $p_1 = 0.230 \pm 0.005$, and then, comparison with Eq. (1) for ID data provides $p_2 = 0.080 \pm 0.005$. Both

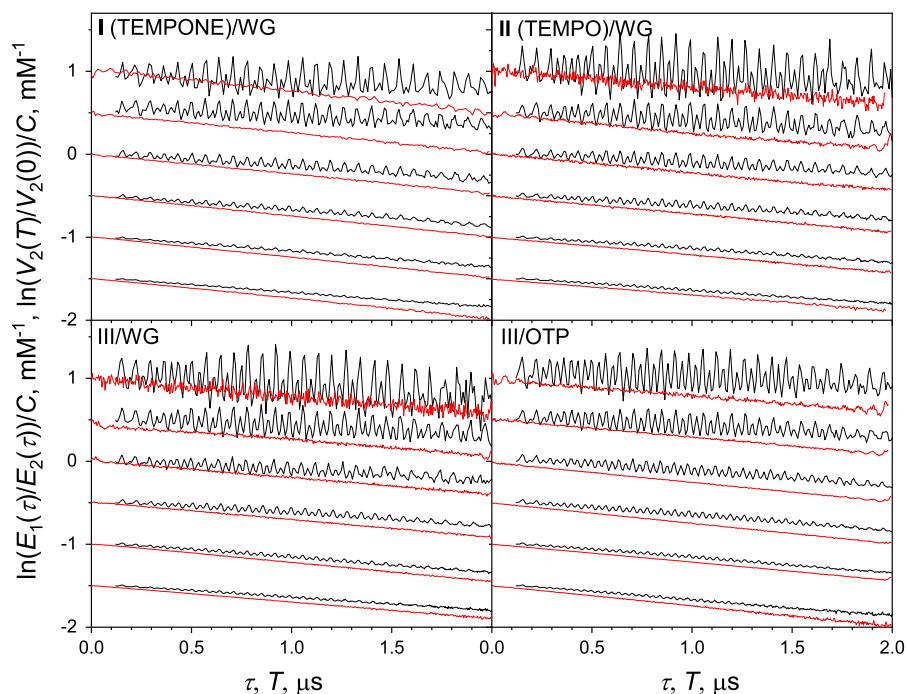


Fig. 4 The semi-logarithmic plot of the ID experiments of the 2nd kind (black curves), and DEER signals (red). All data were divided by concentration C given in mM. The concentrations for each sample are 0.25 mM, 0.5 mM, 1 mM, 2 mM, 4 mM, and 6 mM, from top to bottom (Color figure online)

these values are in reasonable agreement with calculations (not shown) employing Eq. (5).

For small nitroxide concentrations, 0.25 mM and 0.5 mM, the slopes for ID experiment are however relatively small, even close to zero. This implies that, because of relatively weak d–d interaction, another mechanism of echo decay appears. It could be nuclear spin relaxation for the nitroxide ^{14}N nucleus. Indeed, for the central EPR line, this relaxation is twice faster than that for the two side lines [35].

The tangents of the approximation line slopes obtained from data in Figs. 3 and 4 are plotted in Fig. 5. These tangents were obtained for the time intervals up to $2\ \mu\text{s}$ —see Fig. 2b. One can see that tangents for ID and DEER experiments between 1 and 6 mM are almost the same for all studied systems. Such an agreement between ID and DEER data may serve as an additional argument in favor of randomness of spin distribution in the sample under study.

Note that the important source of the data scattering for tangents in Fig. 5 arises mainly from inaccuracy of sample preparation of the desired concentration. This inaccuracy is more noticeable for OTP samples because of high melting temperature and high viscosity.

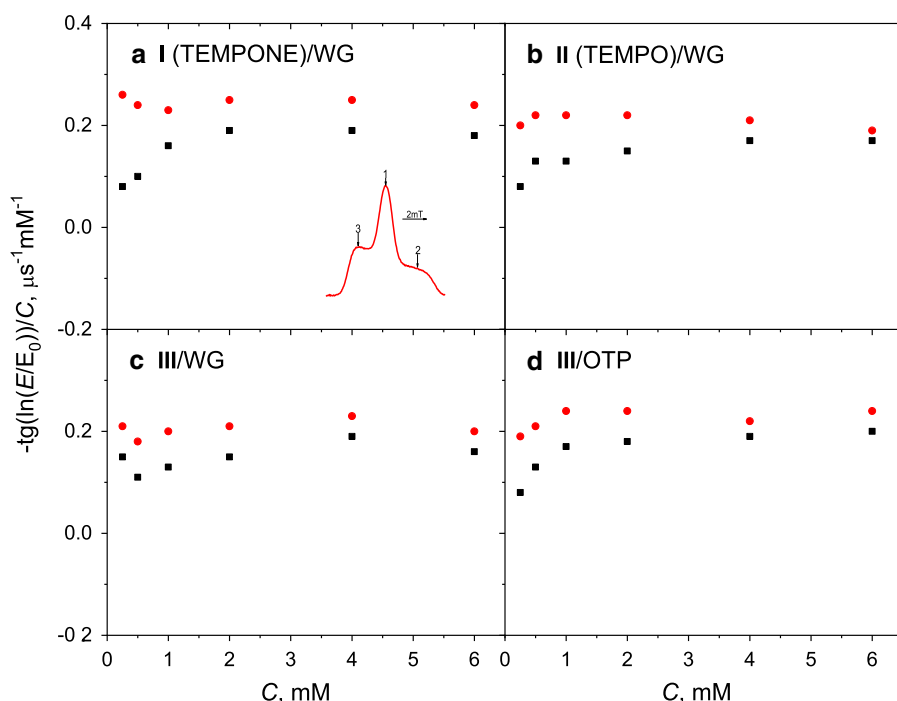


Fig. 5 The tangents of the approximation line slopes for data from Figs. 3 and 4 for ID experiment of the 2nd kind (black squares) and DEER experiment (red circles). Above 1 mM, a standard error approximately matches the symbol size; for lower concentrations, the maximum standard error is $0.05\ \mu\text{s}^{-1}\ \text{mM}^{-1}$ (Color figure online)

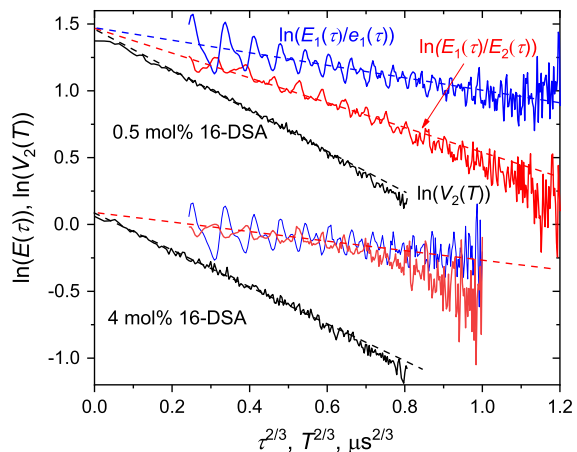
3.2 Spin-Labeled Stearic Acid in DPPC/DOPC Model Membrane

The results of analogous experiments performed on spin-labeled stearic acid (16-DSA) in DPPC/DOPC (1:1) bilayer are presented in Fig. 6. Data are plotted vs. time in the power of $2/3$ – to match the theoretical equations [Eqs. (3) and (4)] for two-dimensional system. Data are given for two 16-DSA concentrations: 0.5 mol% and 4 mol%. (Note that amount of free fatty acids in mammalian membranes varies between 0.3 and 10 mol% [36].) The data in Fig. 6 are arranged in the same way as those presented in Fig. 2b.

One can see that for 0.5 mol%, the data in Fig. 6 resemble those in Fig. 2b: the time dependences for two kinds of ID experiments and the DEER measurements differ in the similar way. However, for the sample with 4 mol % of 16-DSA for the ID experiments of the 2nd kind, the time dependence becomes noticeably weaker. Quantitatively, the tangents of linear dependences in Fig. 6 are 0.46, 0.92 and $1.50 \mu\text{s}^{-2/3}$ for the two kinds of ID and DEER measurements, correspondingly (0.5% 16-DSA), which makes the proportion 0.31:0.61:1, and 0.35, 0.35, and $1.46 \mu\text{s}^{-2/3}$ (4% 16-DSA), which makes the proportion 0.24:0.24:1. Note that for ID experiment of the 1st kind, the found proportions are close to that found from data in Fig. 2b for nitroxides in molecular glasses.

The DEER calibration experiments performed for 16-DSA in methanol-ethanol glass (data not given) allowed to obtain, using Eq. (2), the p_B coefficient. Then, the use of this p_B value (found to be equal to 0.049) in Eq. (4) allowed to obtain the lateral concentration σ_{1oc} of 16-DSA in the membrane. This concentration turned out to be ~ 11 mol%, for both 0.5% and 4 mol% samples. This increase over the average concentration implies that 16-DSA molecules are clustering. The analogous result has been previously found in ID experiment in the membrane for stearic acids spin-labeled at the 5th carbon atom position (5-DSA) [16]. And resemblance of data for 0.5 mol% in Fig. 6 to those given in Fig. 2b implies that ID experiment is capable of obtaining information on local concentration, similar to that given by DEER.

Fig. 6 The same as in Fig. 2b, for 16-DSA in DPPC/DOPC bilayer at concentrations of 0.5 mol% and 4 mol% (shifted along the vertical axis for better presentation). Data are plotted vs. time in the power of $2/3$, to match theoretical equations [Eqs. (3) and (4)] for two-dimensional system. The straight dashed lines are drawn to show these theoretical predictions



To interpret the decrease of the slope of the 2nd kind of ID experiment, we note that previously the analogous effect was found in DPPC/DOPC bilayer for spin-labeled cholesterol analog 3β -doxyl- 5α -cholestane [23]. It was explained suggesting correlation of mutual orientations of the spin labels, because microscopically the $g(\nu_A)$ value in EPR spectrum would be the same for both positions 1 and 2 [23]. So here, we also conclude that orientations in the clusters are correlated. This may be explained by stronger inter-molecular interaction between stearic acid molecules in the clusters upon the concentration increase.

For the 4 mol% 16-DSA, DEER measurements were also performed for different $\nu_A - \nu_B$ offsets. The data obtained are shown in Fig. 7. These data show only slight variation of the time traces with the offset value. This result implies that the so-called orientational selectivity effects [37–39] do not appear in these measurements.

4 Conclusions

DEER signal and ID effect on spin-echo decay are induced by the same physical mechanism that is the modulation of electron spin–spin dipolar interaction by the microwave pulses. So for randomly distributed spin labels, the DEER and ID data are expected to be similar. This similarity was indeed confirmed in this work for the model systems of nitroxides homogeneously dissolved in molecular glasses—for their concentrations up to 6 mM.

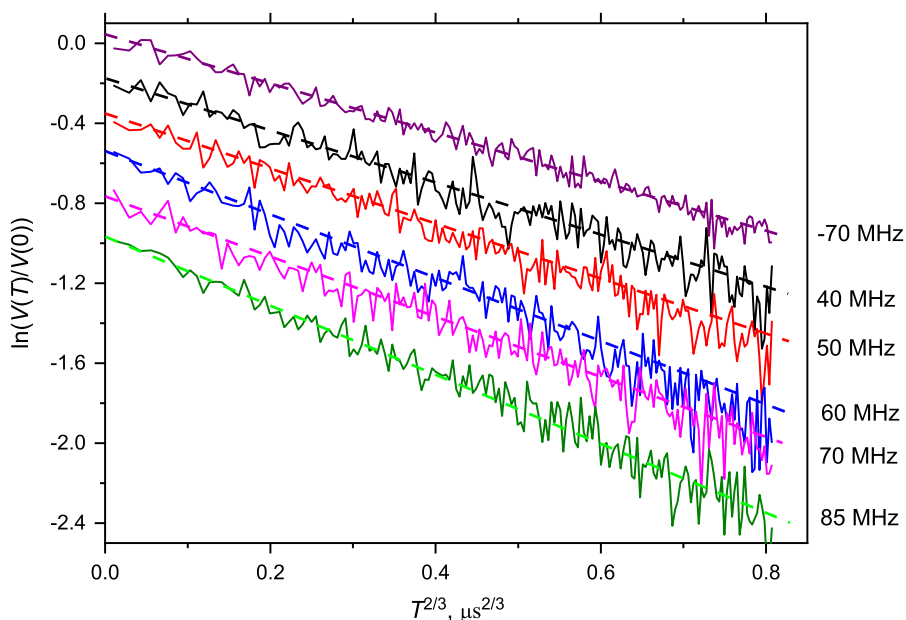


Fig. 7 DEER data for the 4 mol% 16-DSA in DPPC/DOPC bilayer, taken at different $\nu_A - \nu_B$ offsets. The straight dashed lines are drawn to match theoretical prediction of Eq. (4). For convenience, data are shifted along the vertical axis

For spin-labeled stearic acids in a model biological membrane, also studied here, the DEER and ID data demonstrated cluster formation with remarkably enhanced local concentration. Note that these clusters possess a large number of randomly distributed molecules, so that DEER signal decay is consistent with the theoretical prediction given by Eq. (4).

For the high concentration of spin-labeled stearic acids (4 mol%), the ID decay for the 2nd kind of ID experiment was found to be essentially eliminated. This elimination may be explained by mutual correlation of orientations of the nearby spin label. Meanwhile, the ID experiment of the 1st kind is less sensitive to orientational correlation and therefore may be employed for obtaining local concentrations in the clusters.

A comparative study of the DEER signal and the ID effect on spin-echo decay may provide useful information on the mutual locations and orientations of spin-labeled molecules, in the case of their heterogeneous distribution because of clustering.

Acknowledgements Authors are thankful to Dr. D. S. Baranov for his assistance in purification of the substances. This work was supported by the Russian Science Foundation, Project # 21-13-00025.

References

1. A. Milov, K. Salikhov, M. Shchirov, *Soviet. Phys. Solid State* **23**, 565–569 (1981)
2. A.D. Milov, A.B. Ponomarev, Y.D. Tsvetkov, *Chem. Phys. Letters* **110**, 67–72 (1984)
3. M. Pannier, S. Veit, A. Godt, G. Jeschke, H.W. Spiess, *J. Magn. Reson.* **142**, 331–340 (2000)
4. A. Savitsky, K. Möbius, *Photosynth. Res.* **102**, 311–333 (2009)
5. J.P. Klare, H.J. Steinhoff, *Photosynth. Res.* **102**, 377–390 (2009)
6. G.W. Reginsson, O. Schiemann, *Biochem. J.* **434**, 353–363 (2011)
7. G. Jeschke, *Annu. Rev. Phys. Chem.* **63**, 419–446 (2012)
8. T.F. Prisner, A. Marko, S.Th. Sigurdsson, *J. Magn. Reson.* **252**, 187–198 (2015)
9. A. Kuzhelev, D. Akhmetzyanov, V. Denysenkov, G. Shevelev, O. Krumkacheva, E. Bagryanskaya, T. Prisner, *Phys. Chem. Chem. Phys.* **20**, 26140–26144 (2018)
10. X. Bogetti, S. Ghosh, A.G. Jarvi, J.M. Wang, S. Saxena, *J. Phys. Chem.* **124**, 2788–2797 (2020)
11. S. Spicher, D. Abdullin, S. Grimme, O. Schiemann, *Phys. Chem. Chem. Phys.* **22**, 24282–24290 (2020)
12. R. Klaunder, P.W. Anderson, *Phys. Rev.* **125**, 912–932 (1962)
13. K.M. Salikhov, S.A. Dzuba, A.M. Raitsimring, *J. Magn. Reson.* **42**, 255–276 (1981)
14. A.D. Milov, A.G. Maryasov, Y.D. Tsvetkov, *Appl. Magn. Reson.* **15**, 107–143 (1998)
15. G. Jeschke, A. Koch, U. Jonas, A. Godt, *J. Magn. Reson.* **155**, 72–82 (2002)
16. M.E. Kardash, S.A. Dzuba, *J. Phys. Chem. B* **121**, 5209–5217 (2017)
17. A. Raitsimring, in *Biological Magnetic Resonance*, vol. 19, ed. by L.J. Berliner, G.R. Eaton, S.A. Eaton (Kluwer/Plenum Publishers, New York, 2002), pp. 461–491
18. B. Rakvin, N. Maltar-Strmecki, K. Nakagawa, *Radiat. Meas.* **42**, 1469–1474 (2007)
19. M. Marrale, A. Longo, M. Brai, A. Barbon, M. Brustolon, P. Fattibene, *Rad. Meas.* **46**, 789–792 (2011)
20. M. Marrale, A. Longo, A. Barbon, M. Brustolon, M. Brai, *Rad. Protect. Dosimetry* **161**, 398–402 (2014)
21. Y.-C. Lai, A. Chang, C.-M. Yang, Y.-W. Chiang, *Appl. Magn. Reson.* **49**, 1201–1216 (2018)
22. S.A. Dzuba, M.N. Uvarov, D.E. Utkin, F. Formaggio, A. Bedon, A. Orlandin, C. Peggion, *Appl. Magn. Reson.* **48**, 943–953 (2017)
23. M.E. Kardash, S.A. Dzuba, *J. Chem. Phys.* **141**, 211101 (2014)
24. E.F. Afanasyeva, V.N. Syryamina, S.A. Dzuba, *J. Chem. Phys.* **146**, 011103 (2017)

25. S.A. Dzuba, M.E. Kardash, *Biochim. Biophys. Acta Biomembr.* **1860**, 2527–2531 (2018)
26. V.N. Sryamina, N.E. Sannikova, M. De Zotti, M. Gobbo, F. Formaggio, S.A. Dzuba, *Biochim. Biophys. Acta Biomembr.* **1863**, 183585 (2021)
27. I.A. Terracina, M. Todaro, M. Mazaj, S. Agnello, F.M. Gelardi, G. Buscarino, *J. Phys. Chem. C* **123**, 1730–1741 (2019)
28. A.E. London, H. Chen, M.A. Sabuj, J. Tropp, M. Saghayezhian, N. Eedugurala, B.A. Zhang, Y. Liu, X. Gu, B.M. Wong, N. Rai, M.K. Bowman, J.D. Azoulay, *Sci. Adv.* **5**, 2336 (2019)
29. K.M. Salikhov, I.T. Khairuzhdinov, R.B. Zaripov, *Appl. Magn. Reson.* **45**, 573–619 (2014)
30. C.L. Homrighausen, J.A.K. Bauer, *Acta Cryst.* **C55**, 9900102 (1999)
31. E.G. Rozantsev, *Free Nitroxyl Radicals* (Plenum Press, New York, 1970)
32. A.D. Milov, Y.G. Grishin, S.A. Dzuba, Y.D. Tsvetkov, *Appl. Magn. Reson.* **41**, 59–67 (2011)
33. E.P. Kirilina, S.A. Dzuba, A.G. Maryasov, Y.D. Tsvetkov, *Appl. Magn. Reson.* **21**, 203–221 (2001)
34. E.A. Golysheva, G.Yu. Shevelev, S.A. Dzuba, *J. Chem. Phys.* **147**, 064501 (2017)
35. S.A. Dzuba, Y.D. Tsvetkov, *Chem. Phys.* **120**, 291–298 (1988)
36. S. Funari, F. Barcelo, P.V. Escriba, *J. Lipid Res.* **44**, 567–575 (2003)
37. O. Schiemann, P. Cekan, D. Margraf, T.F. Prisner, S.T. Sigurdsson, *Angew. Chem. Int. Ed.* **48**, 3292–3295 (2009)
38. D. Abdullin, G. Hagelueken, R.I. Hunter, G.M. Smith, O. Schiemann, *Mol. Phys.* **113**, 544–560 (2015)
39. C. Abe, D. Klose, F. Dietrich, W.H. Ziegler, Y. Polyhach, G. Jeschke, H.J. Steinhoff, *J. Magn. Reson.* **216**, 53–61 (2012)

Publisher's Note Springer Nature remains neutral with regard to jurisdictional claims in published maps and institutional affiliations.